Current reversal in polar flock at order-disorder interface

Jay Prakash Singh,[1,2,*] Partha Sarathi Mondal,[1,†] Vivek Semwal,[1,‡] and Shradha Mishra[1,§]
[1]*Indian Institute of Technology (BHU), Varanasi 221005, India*
[2]*Israel Institute of Technology Technion, Haifa 3200003, Israel*

(Received 14 February 2023; revised 15 August 2023; accepted 7 September 2023; published 28 September 2023)

We studied a system of polar self-propelled particles (SPPs) on a thin rectangular channel designed into three regions of order-disorder-order. The division of the three regions is made on the basis of the noise SPPs experience in the respective regions. The noise in the two wide regions is chosen lower than the critical noise of order-disorder transition and noise in the middle region or interface is higher than the critical noise. This makes the geometry of the system analogous to the Josephson junction (JJ) in solid-state physics. Keeping all other parameters fixed, we study the properties of the moving SPPs in the bulk as well as along the interface for different widths of the junction. On increasing interface width, the system shows an order-to-disorder transition from coherent moving SPPs in the whole system to the interrupted current for large interface width. Surprisingly, inside the interface, we observed the current reversal for intermediate widths of the interface. Such current reversal is due to the strong randomness present inside the interface, which makes the wall of the interface reflecting. Hence, our study gives new interesting collective properties of SPPs at the interface which can be useful to design switching devices using active agents.

DOI: 10.1103/PhysRevE.108.034608

I. INTRODUCTION

The emergence of collective motion [1–6] and global ordering [7–12] among the various living or nonliving systems, are well-known phenomena. Each particle shows systematic motion at the cost of its internal energy. All individuals in a group synchronize themselves to show different behavioral state, exhibiting a host of interesting properties like pattern formation [13], nonequilibrium phase transition [8], large density fluctuation [14–16], enhance dynamics [17–26], motility-induced phase separation [27–31], etc. Interestingly, different real biological systems are encountered with different kinds of confined geometry [32–36]. Confinement and boundary play significant roles in a variety of biological systems [32], sheared system [37], and other places like fluid dynamics. A boundary can induce many interesting phenomena like, spontaneous flow inside the channel [38], and another classic example includes Rayleigh-Benard convection in the fluid [39,40]. There are a variety of practical applications based on confined geometry like mass transport in nanofluids to enhance the microfluidic devices [41,42], geophysical applications, etc.

There are few studies where researchers have seen the behavior of SPPs at the interface of two different substrate media. Most of the previous studies involve the media of two dissimilar fluids [43–46]. For example, Dirichlet *et al.* [47] observed that catalytic active Brownian microswimmer at different solid-liquid interfaces shows inhomogeneity in the particle speed with respect to the orientation of catalytic substrate at different interfaces. Another well-known conventional example of an interface between superconductor and insulator with boundary is Josephson junction (JJ) in solid-state physics [48–52].

Motivated with the JJ in the solid state, here in this article, we will discuss the collective properties of SPPs by designing a setup analogous to JJ. We have modeled a system of polar SPPs with alignment interaction through a thin rectangular narrow channel. Further, the thin channel is divided into three regions wherein two opposite regions, SPPs move coherently. In the middle region, SPPs diffuse randomly. Although the comparison between our setup and the Josephson junction is not very common since the superconducting phenomena are macroscopically quantum in nature, we still designed an analogous model system for the collection of SPPs and observed the properties of it.

We also studied the case where a small external field is introduced along the long axis of the system, which gives a directional bias for particle alignment. The system is studied for different widths of the intermediate disorder region with and without bias (perturbation). On tuning the width of the disorder region, SPPs with perturbation show a nonequilibrium phase transition, whereas without perturbation, it shows a weak dependence on the interface width. Further, at the junction, particles get reflected from its walls, and we observed the current reversal. This leads some of the SPPs to reorient in the opposite direction and hence contributes to a negative current. The mechanism of reflection due to the interface is microscopically different from the reflection from the hard wall or physical obstacles [53], but on the macroscale, the interaction of an incoming wave of particles in both the cases

*jayps.rs.phy16@itbhu.ac.in
†parthasarathimondal.rs.phy21@itbhu.ac.in
‡viveksemwal.rs.phy17@itbhu.ac.in
§smishra.phy@itbhu.ac.in

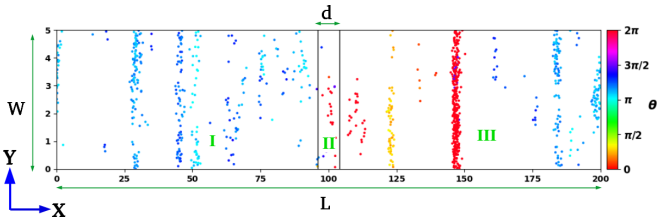

FIG. 1. We show a model picture of the system obtained from the simulation in which different color shows the particle's orientation θ ($\in [0, 2\pi]$). The region II is the interface (junction) with disorder region, whereas the region to the left and right of the interface (I and III) is the ordered region. Noise strength in region II is $\eta_{II} = 0.7$, and in regions I, III $\eta_I = \eta_{III} = 0.3$. d is the width of the interface. The two vertical lines in the middle indicate the boundary of the interface. The W and L are the short and long dimensions of the system. The axis for the two directions of the system is drawn on the left. The asymmetrical geometry of our system becomes evident through the positioning of ticks along the X and Y axis. The periodic boundary condition is used in both directions.

are alike. Finally, we are discussing how the model used here can be utilized for sorting a binary mixture of particles of opposite chirality.

The rest of the manuscript is divided as follows; we have discussed the details of the model in Sec. II. The results are discussed in Sec. III, one possible application in Sec. IV, and the conclusion of the paper with summary is discussed in Sec. V.

II. MODEL

We consider a collection of polar self-propelled particles (SPPs) moving on a two-dimensional substrate on a rectangular narrow channel with periodic boundary conditions (PBC) in both directions. The short and long axes of the channel are denoted by W and L, respectively, as shown in Fig. 1. Particles interact through a short-range alignment interaction within a small interaction radius R_0 [8]. Moreover, the strength of interaction of each SPP is the same. The system is partitioned into three regions: the two regions on the left and right represent the ordered region, and the section in the middle represents the disordered region. The middle disordered region is termed as junction or interface, and the width d of the interface is our tuning parameter. The width of the junction is varied from $d = (0–20)$. In three regions, each particle is defined by its position $\mathbf{r}_i(t)$ and orientation $\theta_i(t)$ at time t and they move along the direction of their orientation with a fixed speed $v_0 = 0.5$. The position and orientation updates of a particle are given by

$$\mathbf{r}_i(t + \Delta t) = \mathbf{r}_i(t) + v_0 \mathbf{n}_i \Delta t, \tag{1}$$

$$\mathbf{n}_i(t + \Delta t) = \frac{\sum_{j \in R_0} \mathbf{n}_j(t) + \eta_{i,k} N_i(t) \xi_i(t)}{w_i(t)}, \tag{2}$$

where $\Delta t = 1.0$ is the unit-time step and $\mathbf{n}_i = (\cos\theta_i, \sin\theta_i)$ is the unit direction vector of the ith particle. In Eq. (2), the first term on the right-hand side represents the short-range alignment interaction inside the interaction radius (R_0) of the ith particle. The second term $\xi_i(t) = [\cos(\phi_i(t), \sin(\phi_i(t))]$ on the right-hand side of Eq. (2) denotes the vector noise, which measures the error made by the particle, following its neighbors. ϕ_i is uniform random angle $\in (0, 2\pi)$, $N_i(t)$ denote the number of neighbors within the interaction radius of the ith particle at time t. Further, $\eta_{i,k}$ ($k = I$, II, and III) ($\eta_I = \eta_{III} = 0.3$ and $\eta_{II} = 0.7$) shows the strength of the randomness present in the system for the three regions. We choose the mentioned values of noise because, for the clean polar SPPs interacting through Vicsek type alignment interaction with vector noise, the order-disorder transition occurs at $\eta \sim 0.6$ (for the same set of parameters used here) [14,54]. $w_i(t)$ is the normalization factor which reduces the right-hand side of the Eq. (2) to a unit vector. We named the model above as the system without perturbation (WOP).

We also introduced an external perturbation along the long axis of the channel. It gives a directional bias for the SPPs motion; hence, the orientation update equation will become

$$\mathbf{n}_i(t + \Delta t) = \frac{\sum_{j \in R_0} \mathbf{n}_j(t) + h_0 \mathbf{n}_\mathbf{p} + \eta_k N_i(t) \xi_i(t)}{w_i(t)}, \tag{3}$$

where h_0 is the strength of the external field and is kept fixed to a small value with direction $\mathbf{n}_\mathbf{p} = (1, 0)$. Using Eq. (3), the model is referred to as system with perturbation (WP). Further, the number density of SPPs is defined by $\rho = \frac{N}{L \times W} = 1.0$, where N is the total number of particles in the system. All the particles are allowed to move throughout the system, and they experience the noise of different regions accordingly. We let the system evolve from a random homogeneous state of density and orientation of particles. All the results discussed below are in the steady state, and the total time step of the simulation is taken 10^6. One simulation step is counted after the update of all the particles once. Numerical details and parameters are chosen as $R_0 = 1.0$, $L = 200$, $W = 5$, and h_0 is varied from 2% to 6% of the strength of alignment. A total of 20 to 200 independent realizations are used for better statistics.

III. RESULTS

A. Global ordering and junction width (d)

First, we study the effect of junction width d on the global orientation in the whole system of size $L \times W = 200 \times 5$. Ordering in the system is characterized by the orientation order parameter,

$$\Psi(t) = \frac{1}{N} \left| \sum_{i=1}^{N} \mathbf{n}_i(t) \right|. \tag{4}$$

In the ordered state, i.e., when the majority of particles are moving in the same direction, then Ψ will be closer to 1, and of the order of $\frac{1}{\sqrt{N}}$ for a random disordered state. First, we show the variation of $\Psi = \langle \Psi(t) \rangle$, where $\langle .. \rangle$ means average over time in the steady state and over 20 independent realizations. We first study the system WOP. In Fig. 2(a), we plot Ψ versus junction width d and found that with an increase in d, Ψ shows small decay, which is further confirmed by the orientation probability distribution function (PDF) $P(\Psi)$ in Fig. 2(b). To understand the small decay of Ψ with width d, we have shown the snapshots for two different junction widths $d = 2$ and 18 in Figs. 2(c) and 2(d), respectively. The position

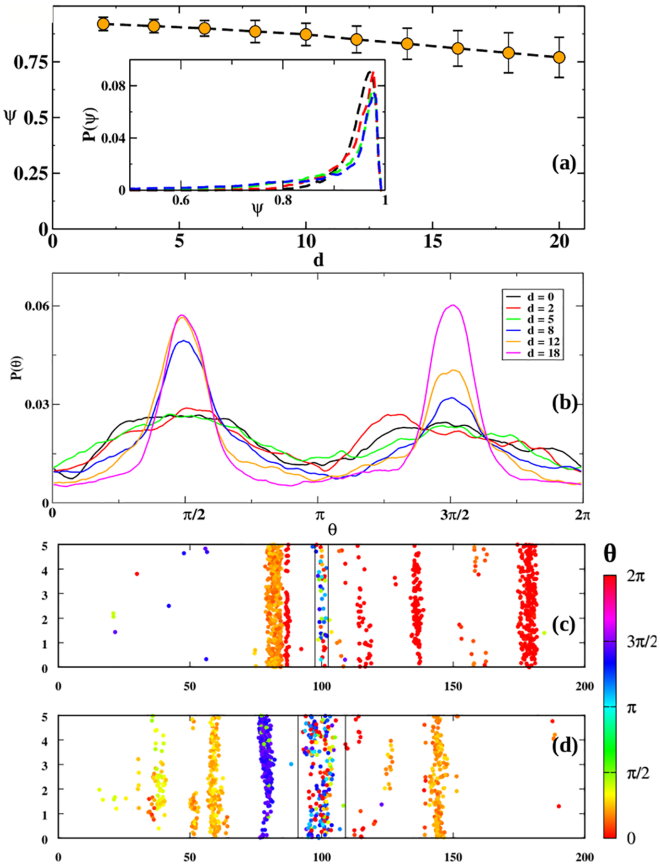

FIG. 2. All the plots (a)–(d) shown here for WOP. (a) Plot of global orientation order parameter Ψ vs width of the disorder region d. Panel (a) shows the global order parameter distribution $P(\Psi)$ for different widths of the junction d. Different colored break lines are for $d = 4$ (black), $d = 8$ (red), $d = 12$ (green) and $d = 18$ (blue). (b) Probability distribution of particles angle, $P(\theta)$ for ($d = 0$) and different widths of interface. Panels (c, d) show the snapshots of the system for widths $d = 5$ and $d = 18$, respectively. Color of each particle represents its orientation θ ($\in [0, 2\pi]$) according to the color bar. $L \times W = 200 \times 5$ and $\rho = 1.0$. Note that the aspect ratio of the box shown in panels (c, d) is not the same as the actual aspect ratio of the system. Hence, tics on both axes are important. This is true for all the color plots shown later.

of the particles are represented by circles, and their color represents the orientation of the particles. In general, the SPPs form the ordered band inside the ordered region as shown by the dense moving SPPs along the channel in Fig. 2(b) (from the right direction). The size of the ordered band or cluster depends on the chosen set of system parameters [14,55]. For the typical choice of parameters in this work, it is approximately 10.

In the snapshots shown in Figs. 2(c) and 2(d) and animations in SM1_I [56] and SM1_II [56], the cluster of particles, which look like a band is actually a manifestation of the very small transverse Y dimension of the system. Hence, what seems like a band in our figures and animations is basically a cluster of size greater than the transverse dimension of the system. The direction of motion of the ordered cluster is the same as reported in previous literature [14]. To quantify the direction of an ordered cluster, in Fig. 2(b) we show the probability distribution of the particles angle $P(\theta)$, averaged over 200 ensembles for different widths ($d = 0$–18) of the interface. For zero interface $d = 0$, the distribution is broad with some structures due to periodic boundary conditions in both directions. For small interface widths $d \leqslant 5$, the $P(\theta)$ starts to develop multiple minor peaks. For larger interface widths $d \geqslant 8$, the particles start to avoid the interface, and it encourages the dynamics of particles in $\pm Y$ direction, and the probability distribution starts to develop peaks at $\pi/2$ and $3\pi/2$. But due to the presence of finite noise, a small X-component is also present, and hence a moving cluster possesses a nonzero velocity in the X-direction, and they will encounter the interface.

Now we discuss the interaction of a moving cluster with the interface. For small widths: the width of the interface is smaller than the size of the cluster, and the SPP passes the interface before it experiences the disorder present inside the interface [as shown in Fig. 2(c)]. Hence, the global order parameter retains a high value ~ 0.8, and the direction of moving SPPs remain unaffected after interaction with the interface [shown by the almost clear common orientation of all particles in the system in Fig. 2(c)].

As we increase the width of the interface to a size larger than that of the particle cluster, an interesting phenomenon occurs during the interaction. Before the cluster can completely pass through the interface, it encounters disturbances at the interface, causing the front of the cluster to randomize. This randomization affects the particles at the back as well, leading to a partial reorientation of the cluster before passing through, as depicted in Fig. 3(a)(I–II). The entire process appears akin to a reflection due to the presence of the interface, as shown in Fig. 3(a)(III–IV). While a portion of the cluster successfully emerges from the other side, contributing to the forward moving current, a finite fraction of particles experience reflection from the interface walls, as observed in Fig. 3(a)(V–VI).

To better understand this behavior, we analyze one-dimensional density, $\rho(x)$, and the X component of velocity, $\langle v_x(x)\rangle$, averaged over the transverse direction, as presented in Figs. 3(b) and 3(c), respectively. Initially, as shown in (I) and (II), the band approaches the interface with a positive $\langle v_x(x)\rangle$. However, upon entering the interface, the cluster experiences significant fluctuations in $\langle v_x(x)\rangle$ around zero, indicating randomization and resulting in the splitting of the band. Eventually, one part of the band reverses its direction and emerges from the interface, showing distinct characteristics of reflection. The interaction between the moving cluster and the interface is effectively demonstrated through an animation in SM1_I [56] using the same parameter values as depicted in Fig. 3. The interface acts like a partially reflecting wall, compelling the self-propelled particles (SPPs) to avoid the junction and exhibit intriguing behavior during the process. In the snapshots illustrated in Fig. 3(a), as well as in the corresponding system animation labeled as SM1_I [56], a cluster of particles exhibits movement in the $+ve\ X$ direction, converging upon the interface from the left side. In the particle orientation probability distribution depicted in Fig. 2(b), we assert that particle motion, including that of the cluster, is unbiased along the X direction for the case WOP. To substantiate our claim, we have included an additional animation employing the identical parameter values as those presented in

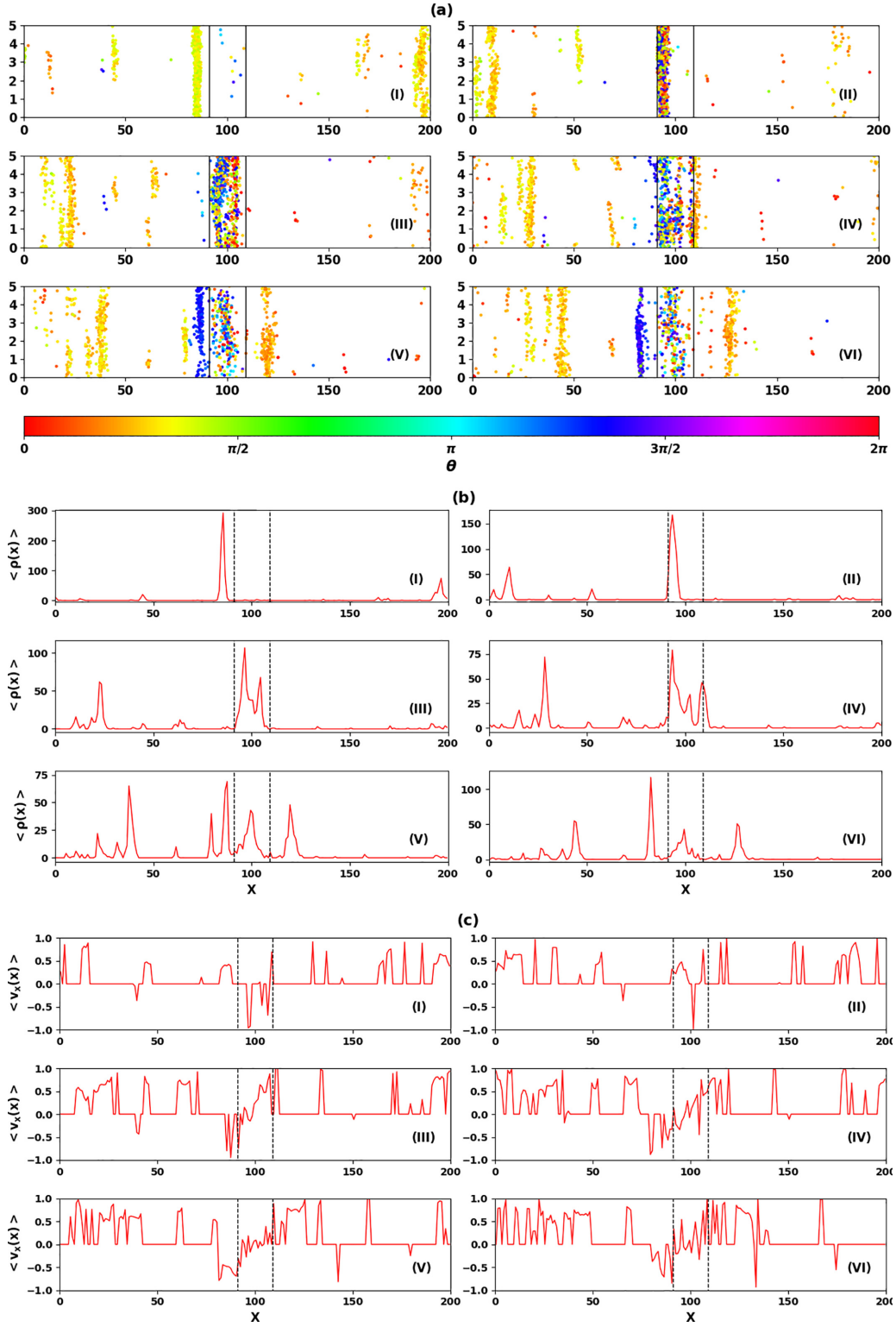

FIG. 3. The figure depicts the reflection of a particle cluster from the interface in the WOP case for interface width, $d = 14$. The chosen times highlight a dense cluster (band) of particles moving towards the interface, clearly visible in subplot (I) and discernible through the color bar. Subsequent plots in panels (a)–(c), each with six subplots (I–VI), showcases the evolution of various quantities at specific times: $t = 2122$, 2163, 2204, 2223, 2253, and 2271, respectively. In each subplot of panel (a), particle orientation angle θ is represented by the color of particles, as shown in the color bar. Subplots in panel (b) display the one-dimensional density $\langle \rho(x) \rangle$ averaged over the transverse direction, while subplots in panel (c) exhibit the coarse-grained one-dimensional $X-$ component of velocity $\langle v_x(x) \rangle$ of particles averaged over the transverse direction. Throughout all subplots of panel (a), two vertical black lines mark the position of the interface. Additionally, the tick labels along the X and Y directions of the system reveal significant anisotropy in the system's geometry. In panels (b, c), black vertical dashed lines indicate the interface's position along the X-direction. The interface's width is denoted by $d = 14$, and all other parameters remain consistent with those in Fig. 2.

Fig. 3, denoted as SM1_II [56], which portrays the interaction of particles with the interface and showcases the phenomenon of reflection from the interface. Notably, in this animation, the cluster demonstrates motion in the $-ve$ X direction, approaching the interface from the right side. This presentation effectively underscores our conclusion that the occurrence of reflection from the interface remains consistent, irrespective of the direction from which the cluster approaches.

The current reversal from the interface appears due to the sudden temperature difference in our present model. It is simply due to the interaction of an incoming wave of particles with the interface. When an incoming wavefront experiences an abrupt change in thermal noise, the front of the wave gets randomized, and that information very soon passes to the particles at the back of the wave. They start to reorient in different directions, and by orienting in the direction opposite to the direction of motion of the wavefront, they have a better probability of leaving the interface soon and forming another cluster moving in the opposite direction. The whole mechanism acts like a reflection from the interface. This mechanism is microscopically different from the reflection due to a physical obstacle; if we place an obstacle in the direction of a moving particle, as a result of interaction with the obstacle, the particle experiences a torque due to the walls of the obstacle and the direction of the particle gets reoriented. This is true for a single particle. However, if a wave interacts with the walls of the obstacle, then a fraction of particles of the wave get reoriented due to the interaction with the wall and then slowly accumulate more and more particles with them and leading to the formation of a wave moving in opposite direction and mechanism is like reflection. Hence, we argue that, although the mechanism of reflection due to the interface is microscopically different from the reflection from the hard wall or physical obstacles [53], on the macroscale, the interaction of an incoming wave of particles in both the cases are similar.

The periodic boundary condition gives rise to multiple instances of the reflection process, and in the long run, particles start avoiding the interface. Hence, their orientation develops contributions in Y direction represented by $P(\theta)$ plot for $d = 8$ and 12 in Fig. 2(b). As shown in the snapshots Fig. 3(a)(V–VI), the orientation of particles are not along the $\theta = (0, \pi,$ or $2\pi)$. This reduces their frequency of entering the interface. This results that mostly the SPPs are moving in the ordered region only, and we find weak dependence of the global order parameter on the width d.

Further, we have studied the system WP. The perturbation is introduced in such a way that the flock is biased to move along the $+ve$ direction of the long axis (x axis). Interestingly, we have found that global orientation order parameter Ψ decay sharply with an increase in the junction width d as shown in Fig. 4(a), Which has been confirmed by plotting the probability distribution function (PDF) $P(\Psi)$ for different junction widths d as shown in the inset of Fig. 4(a).

Figures 4(b) and 4(c) show the snapshots for two different junction widths $d = 5$ and 18. Due to a finite perturbation along the $+ve$ X direction, a moving flock can easily enter inside the junction from the left wall. For lower widths of the junction, the flock does not experience any hurdle and passes coherently, resulting in higher values of Ψ. Moreover,

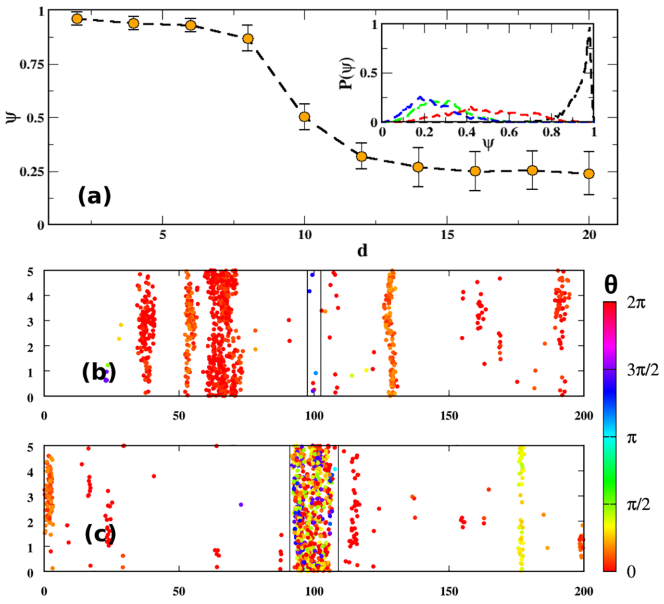

FIG. 4. All the plots (a)–(c) shown here for WP ($h_0 = 2\%$). (a) The plot of global orientation order parameter Ψ vs width of the disorder region d. Panel (a) plot shows the global order parameter distribution $P(\Psi)$ for different widths of the junction d. Different colored break lines are for $d = 4$ (black), $d = 8$ (red), $d = 12$ (green), and $d = 18$ (blue). Color of each particle represents its orientation θ ($\in [0, 2\pi]$) according to the color bar. Plots (b) and (c) show the snapshots of the system for width $d = 5$ and $d = 18$, respectively. The other details of the parameters are the same as in Fig. 2.

for higher junction widths, we find a dense cluster of SPPs inside the junction with random orientations, resulting in the decrease of the value of Ψ. The same can be explained by the plot of the probability distribution of the fraction of particles $P(f)$ inside the junction as shown in Fig. 8(b). This is very different from what we observed for system WOP as shown in Figs. 2(d) and 3, where the boundary of the interface acts like partially reflecting walls. But for the system WP, due to a directional bias, the moving band of SPPs is forced to enter inside the interface. Inside the interface, the strength of the external perturbation is not strong enough to help them to pass. But it resists their orientation in the opposite direction. It leads to the accumulation of particles inside the junction as shown in Fig. 4(c) and results to the small order parameter for large junction width d.

In Figs. 5(a)–5(c) (snapshots, one-dimensional density $\rho(x)$ and $\langle v_x(x)\rangle$, respectively), we illustrate the interaction of a moving band with the interface at different times. Initially, the band exhibits positive $\langle v_x(x)\rangle$, indicating the band is moving towards the interface for the current position of the band as shown in Figs. 5(a)–5(c) (I–II). However, upon encountering the interface, the band experiences fluctuations from the interface Figs. 5(a)–5(c)(III–IV), which tends to randomize the cluster. Despite strong randomness within the interface, the driving force along $+X$ prevents a significant negative $\langle v_x(x)\rangle$. As a consequence of the interplay between the driving force and the intense randomness, the particles remain entrapped within the interface for a prolonged period and come out of the other side of

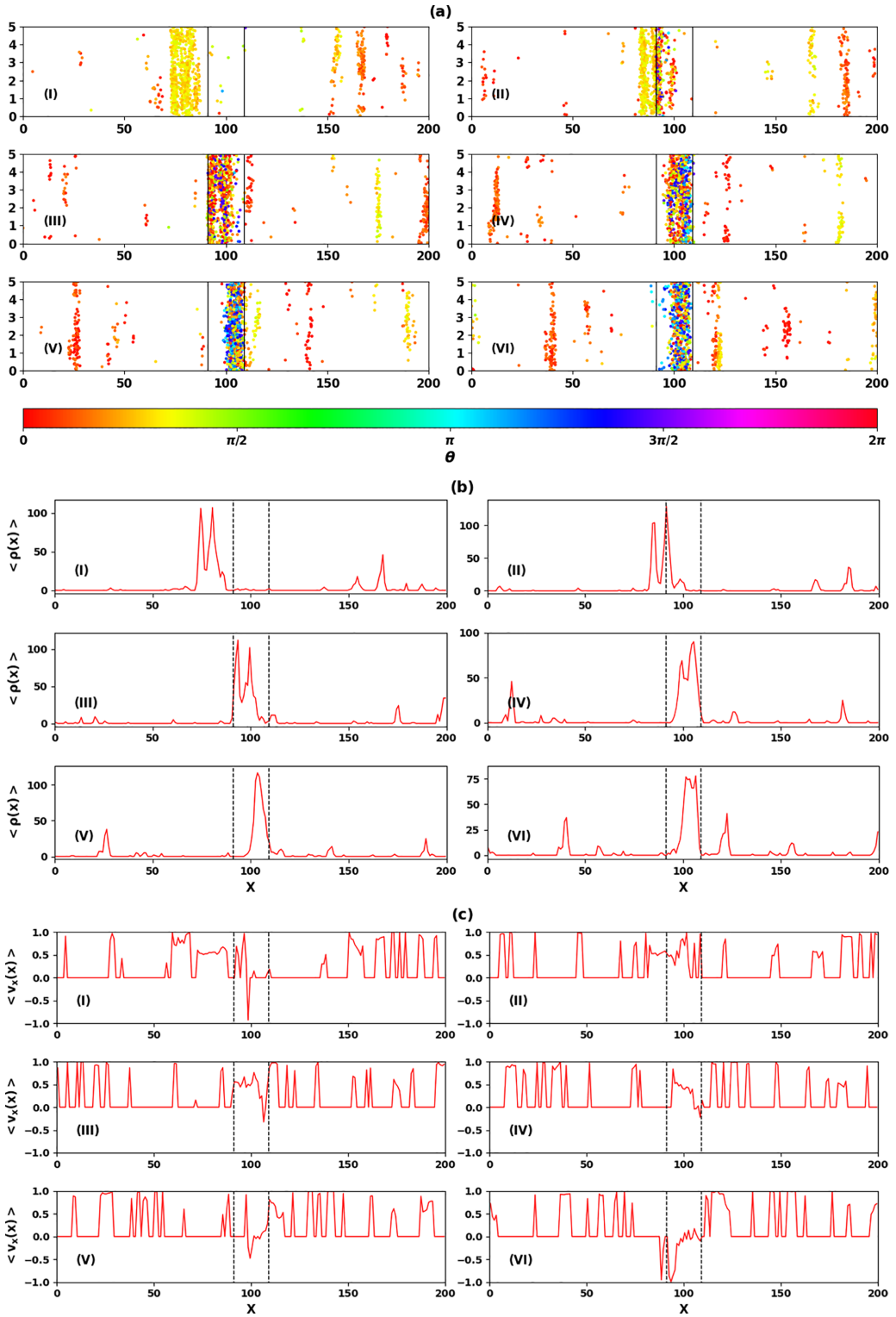

FIG. 5. This figure illustrates the absence of reflection from the interface in WP case for interface width, $d = 14$. The first subplots, (I), in panels (a)–(c) show a cluster approaching the interface. Consecutive snapshots show the evolution of various quantities at later times, $t = 2670$, 2710, 2740, 2770, 2800, and 2830, respectively, from (I–VI). In each subplot of panel (a), the particle orientation angle is represented by their colors, as shown in the color bar. Subplots in panel (b) display the $\langle \rho(x) \rangle$, while subplots in panel (c) exhibit $\langle v_x(x) \rangle$. All other parameters and details remain consistent with those in Figs. 2 and 3.

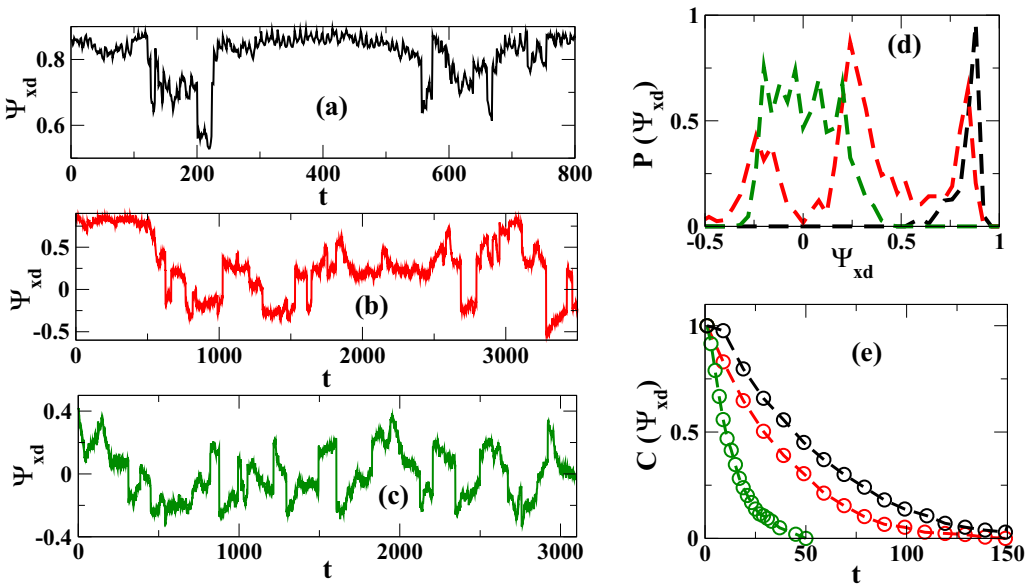

FIG. 6. Plots (a)–(c) show the time variation of event current Ψ_{xd} along the long axis with increasing width d. (d) Event current distribution $P(\Psi_{xd})$. Panel (e) shows the X-orientation current autocorrelation for three junction width d. Black, red, and green colors show the results for junction widths $d = 4$, 8, and 12, respectively. The other parameters are the same as in Fig. 2

the interface with a positive value of $\langle v_x(x)\rangle$ as shown in Figs. 5(a)–5(c)(V–VI). Thus, no clear reflection of particles from the interface is observed here. The details of the interaction of a band with the interface for system WP are shown in SM2 [56].

B. Current inside the junction

1. Junction current

In this section, we discuss the junction current within the junction along the long X axis as well as Y axis with the variation of the junction width d for WOP. The junction current is calculated when at least 25% particles of the whole system are within the junction, and we named this current as event current. The event current in the junction along X and Y directions is defined by $\Psi_{xd}(t) = \frac{1}{N_1}\sum_i^{N_1} n_{xi}$, $\Psi_{yd} = \frac{1}{N_1}\sum_i^{N_1} n_{yi}$. The n_{xi}, n_{yi}, and N_1 represent the components of the velocity vector along the long and short axis, and the total number of particles within the junction, respectively. In Figs. 6(a)–6(c), we show the time series of Ψ_{xd} for different values of junction width d. We observe, with increased d, the amplitude of Ψ_{xd} decreases and also positive and negative current changes in a periodic fashion with the decreased period. Here current is carried by the particles along $+ve$ and $-ve$ X direction; we call them positive and negative currents, respectively. Further, in Fig. 6(d) we show the current probability distribution function $P(\Psi_{xd})$ of Ψ_{xd}. It clearly suggests that with the increase in the width of the junction, there is a clear signature of the current reversal. Also, in Fig. 6(e) we plot the current-current autocorrelation function (CACF) $C_{(\Psi_{xd})}(t) = \langle \Psi_{xd}(t_0) \cdot \Psi_{xd}(t + t_0)\rangle$, where $\langle ..\rangle$ represents the average over many ensembles and reference time t_0. The autocorrelation function decay sharply by increasing junction width d. Hence, we find that in the channel, the current along the long axis alternates from $+ve$ to $-ve$ on tuning the width d. Our claim regarding the current reversal phenomena is a very interesting property of the flock at the junction. For small widths $d < 8$, a coherent flock enters into the junction and crosses without significant deviation. For intermediate widths $8 \leqslant d \leqslant 16$, we observed that once coherent moving SPPs enter the junction, it faces randomness inside the junction. Since inside the junction, all the directions are equally probable, but the flock prefers to move in $+ve$ or $-ve$; X direction, which leads to a quicker escape from the disorder region. Further SPPs try to come out from the junction and perform back and forth oscillations within the junction. These oscillations are termed as alternating event current. Interestingly this oscillation is more prominent for the intermediate junction widths $8 \leqslant d \leqslant 16$. For small widths of the junction, the length of a moving band of SPPs is of the order or larger than the width of the interface, and SPPs can easily pass through it with small disturbance; hence the X current Ψ_{xd} shows small oscillations with time and no negative current. But as we increase the width of the interface, when the size of the interface is larger than the size of the ordered band, then for some distance, the moving band of SPPs is able to penetrate (which is analogous to the penetration depth in solid state) and then experience randomness. This leads to a fraction of particles from the moving band reversing its direction of motion and we experience a negative current, and hence negative Ψ_{xd} as shown in Figs. 6(b) and 6(c). Increasing the interface width, the frequency of alternating current increases, which leads to the sharper decay of the CACF $C_{(\Psi_{xd})}(t)$ shown in Fig. 6(e). This leads to the phenomena of current reversal inside the junction. For widths $d > 20$, moving SPPs experience more and more reflection and are unable to enter inside the junction and get reflected from the wall itself; hence, we have a weak junction current. Due to that, the magnitude of the junction current Ψ_{xd} decreases with increasing d.

Furthermore, in Figs. 7(a)–7(c), we show the junction current in Y direction Ψ_{yd} and current PDF $P(\Psi_{yd})$ along the

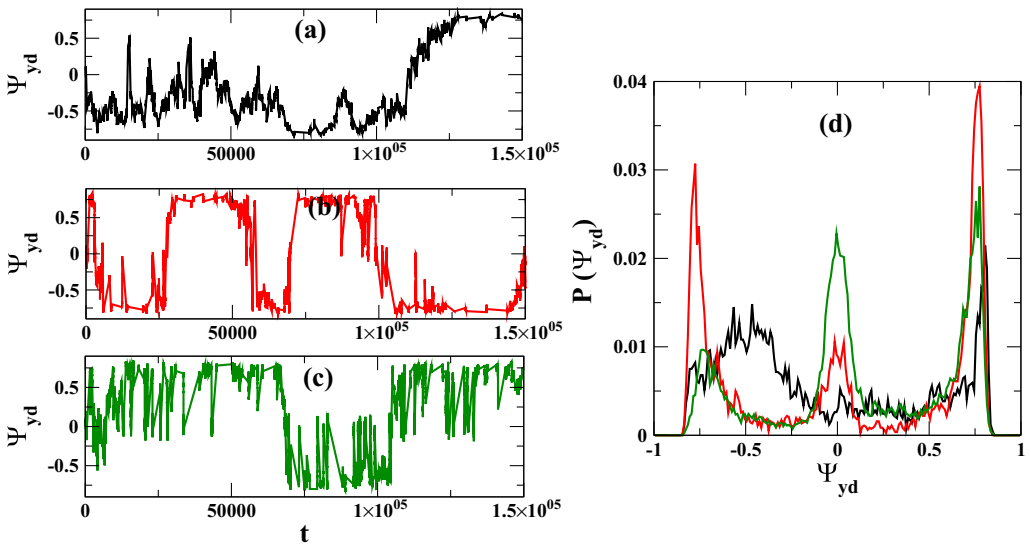

FIG. 7. Plots (a)–(c) show the time variation of orientation event current Ψ_{yd} along the short axis with increasing width d. (d) Orientation event current distribution $P(\Psi_{yd})$. Black, red, and green colors show the junction width $d = 4$, 8, and 12, respectively. The other parameters are the same as in Fig. 2

small axis versus junction width d. We observe the oscillations in Ψ_{yd} too, but the timescale of oscillations is much larger than those for Ψ_{xd} and are not due to the current reversal in Y direction. Such periodicity is further confirmed by the current distribution $P(\Psi_{yd})$ is shown in Fig. 7(d).

C. Fraction of particles inside the junction

Until now, we have discussed the orientation of moving SPPs inside the junction. We also find interesting results for the fraction of particles inside the junction $f(t) = \frac{\mathcal{N}(t)}{N}$. Here $\mathcal{N}(t)$ is the number of particles inside the junction at time t. We compared the probability distribution function (PDF) of $f(t)$ for the systems WOP and WP. The PDF, $P(f)$, is obtained by calculating the normalized distribution of the fraction of particles inside the junction, and then PDF is averaged over different independent realizations.

In Figs. 8(a)–8(d) we show the plot of $P(f)$ versus f for different junction widths ($d = 4$–20) for different strengths of perturbations 0% (WOP), 2%, 4%, and 6%, respectively. For all the cases the, tail of the distribution extends on increasing width of the interface d, due to the increased area of the interface and hence more number of particles inside the junction. For all junction widths, the PDF is a power law with slope $f^{-1.25}$ for system WOP [as shown by log - log plot in the main plot of Fig. 8(a)]. It suggests the probability of finding all possible values of f for system WOP. The inset Fig. 8(a) shows the same plot on log -y scale to compare that the distribution is clearly a power law and not an exponential. For the system WP, the distribution clearly has a deviation from power law and shows a clear peak for f close to 1 as shown in Figs. 8(b)–8(d). The height of the peak increases on increasing width d. For larger widths and small perturbation (2%) [Fig. 8(b)], a macroscopic fraction of particles if present inside the junction. The appearance of a peak close to $f \simeq 1$ is visible more clearly in the inset plot of Fig. 8(b), which is shown on the log -y scale. As we increase the perturbation further, the peak at larger f starts to weaken, and distribution flattens for intermediate $f's$. It starts to appear more exponential in nature for larger perturbations $\geqslant 4\%$ as shown in the insets of Figs. 8(c) and 8(d), which are drawn on log -y scale. The exponential nature of the tail of the distribution represents a critical fraction of particles inside the junction. For 6% perturbation [Fig. 8(d) (main figure)], the distribution shows a power law decay with power f^{-1} for moderate $f's$. It suggests a moderate fraction of particles inside the junction.

Here we summarize the behavior of the density of particles inside the junction. Adding a finite perturbation eases the SPPs to get into the interface. For weak perturbation, although perturbation is enough for SPPs to enter the junction, but not sufficient for them to overcome the randomness present there. This lead to the accumulation of particles inside the junction, and $P(f)$ shows a peak at $f \simeq 1$. As we increase the perturbation, it guides the quicker entry of SPPs to the junction, but now perturbation is comparable to the randomness present inside, which results in the flattening of the $P(f) \simeq f^{-1}$ for higher perturbations.

Until now, we discussed the effect of the model introduced here on the properties of SPPs. Now we come to one good application of our model. In Sec. IV, we give an example showing how the junction can be used for sorting two types of particles with different chirality.

IV. JUNCTION AS A PARTICLE SORTER

In this section, we propose that such geometry of the system for the case WOP can also be used for the sorting of two types of particles. As described earlier and clearly visible in the animation SM1_I [56] and SM1_II [56], for low and intermediate junction widths, a part of the incoming cluster of particles crosses the junction, and some of the particles get reflected from the walls. Due to the periodic boundary condition, with time, a cluster splits into many smaller clusters

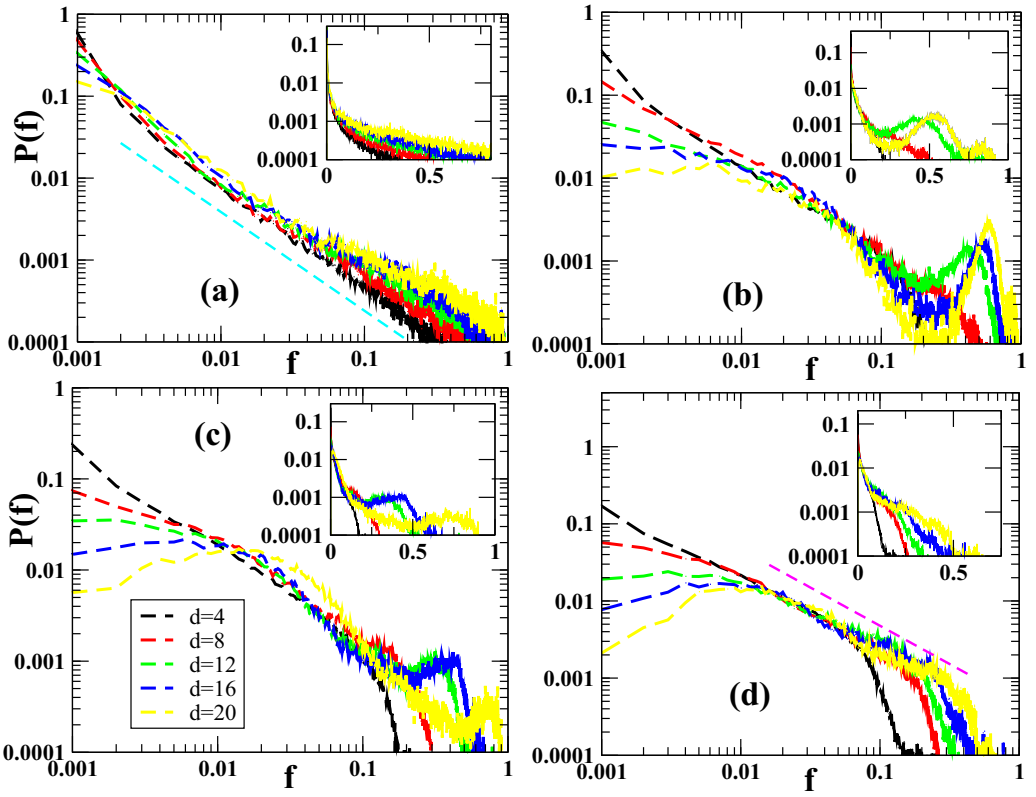

FIG. 8. Probability distribution, $P(f)$, inside the junction: Plot (a) is for WOP case and plots (b), (c), (d) are for WP case with perturbation strength (h_0) 2%, 4%, and 6%, respectively, on log-log scale. Colors black, red, green, blue, and yellow correspond to $d = 4$, 8, 12, 16, and 20, respectively. Insets show the plot of $P(f)$ vs f in log -y scale. In plot (a), the dashed line (cyan) is the power law with exponent 1.25, and in plot (d) dashed line (magenta) is the power law with exponent 1. Other parameters are the same as in Fig. 2

and starts to develop preferential motion in the Y direction, as shown by $P(\theta)$ plot in Fig. 2(b) for $d = 8$ and 12.

This motivated us to think: What will happen if we place a mixture of two different types of particles in the system? To investigate that, we considered a mixture of two types of particles (1 and 2) with *left* and *right* chiral, respectively. Both types of particles are distributed with random orientation and position in the system. We expect the particles with left chirality will prefer to be reflected from the left wall, and right chirality will have the ease to transmit the interface for an incoming cluster coming from the region I and vice versa.

The difference in chirality is introduced by their response to the random vector noise $\phi \in (-1.1\pi, +0.9\pi)$ for the first type and $\phi \in (-0.9\pi, +1.1\pi)$ for the second type. Hence, one type of particle has noise with a mean -0.1π, and the noise has a mean 0.1π for the second type.

Also, the strength of alignment interaction is much stronger for particles of its own type compared to the other type (1.0 and 0.5, respectively). We begin with an initially homogeneous mixture of two types of particles. The results reveal that over time, the particles undergo phase separation, leading to the formation of distinct clusters. In Fig. 9, we present the phase separation process for an interface of width $d = 12$, showing steady-state snapshots in Fig. 9(a) and the one-dimensional density, $\langle \rho(x) \rangle$, of the two particle types in Fig. 9(b), represented by red and blue colors, respectively. Subplots (I–VIII) correspond to progressively increasing time intervals. In subplot Figs. 9(a) and 9(b)(I–III), the particles are dispersed to some degree, indicating the presence of a demixed phase. However, as time progresses, the particles begin to phase separate, forming bands on two sides of the interface, as demonstrated in Figs. 9(a) and 9(b)(IV). Once the phase separation occurs, the system maintains this configuration for some time as depicted in Figs. 9(a) and 9(b)(V–VI), after which the bands start to disperse [Figs. 9(a) and 9(b)(VII–VIII)], ultimately leading to the formation of the mixed state once again. This cyclic process of mixing-demixing-mixing continues, resulting in an intriguing dynamic interplay of the particle clusters within the mixture.

To characterize this phenomenon, we define the phase separation order parameter as

$$p(d) = \frac{1}{N} \sum_{i=1}^{N} \left| \frac{N_1(i) - N_2(i)}{N_1(i) + N_2(i)} \right|, \tag{5}$$

where $N_{1,2}(i)$ are the number of particles of type 1 or 2 in the neighbourhood of ith particle. p has a value close to 1 if the same types of particles are together or when they are demixed and close to zero for a perfectly mixed situation. In Fig. 9(c)(I–IV), we present time series data for $p(d)$, illustrating four distinct interface widths: $d = 5$, 8, 14, and 18, respectively. This visual representation effectively elucidates the observed patterns of mixing, demixing, and subsequent mixing between the two types of particles

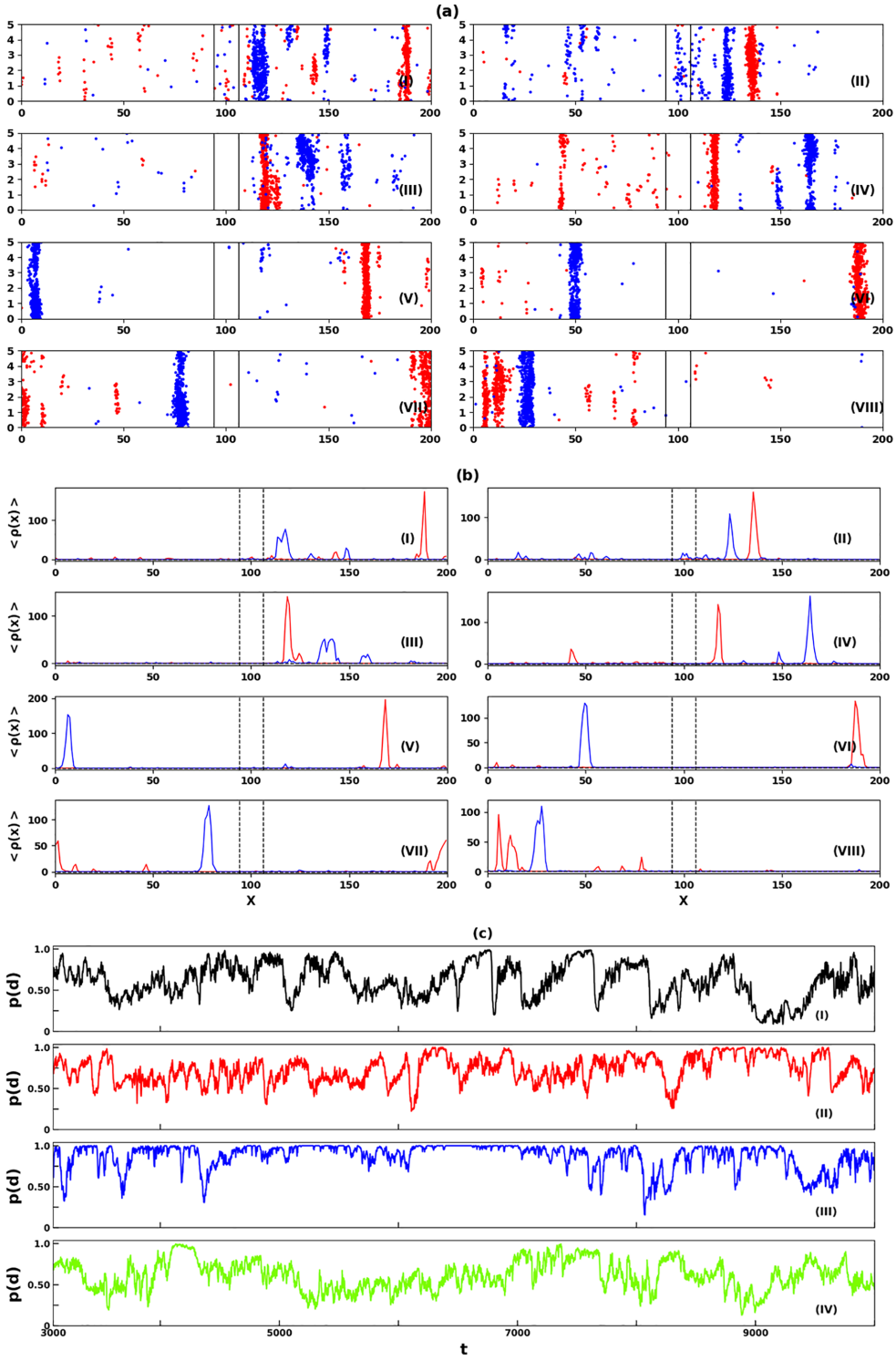

FIG. 9. This figure illustrates the phase separation of two types of particles with different chirality for a width parameter $d = 12$, presented as snapshots in panel (a), and the one-dimensional density averaged, $\langle \rho(x) \rangle$, over the transverse direction, as shown in panel (b). The subplots (I–VIII) in panels (a) and (b) display the system's evolution at subsequent times: $t = 2440$, 2850, 3000, 3370, 3650, 3935, 4100, 4500, respectively. In subplots (I–VIII) of panel (a), particles of two different chirality are depicted with distinct colors (red and blue). The two vertical black lines indicate the interface between the two phases. Additionally, the tick labels along both axes highlight the strong asymmetry in the geometry of the system. In subplots (I–VIII) of panel (b), two different colors are used to represent the two different types of particles, consistent with panel (a). Black vertical dashed lines are utilized to indicate the position of the interface along the long direction only; subplots (I–IV) in panel (d) present time series data of the phase separation order parameter, denoted as $p(d)$, for four specific values of d: 5, 8, 14, and 18, all obtained from a single ensemble. All other system details remain the same as in Fig. 3.

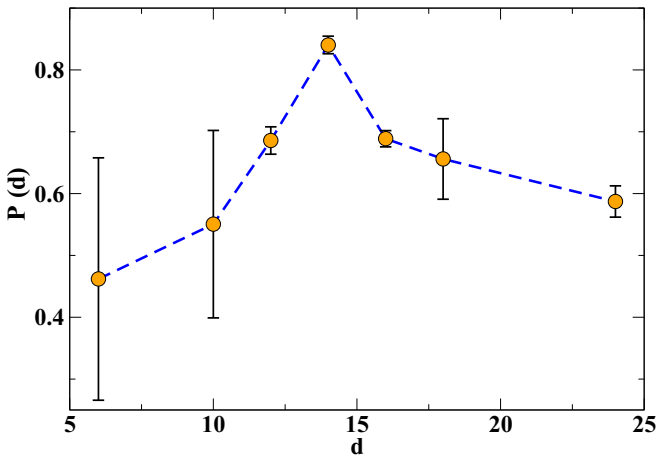

FIG. 10. Plot of phase separation order parameter $P(d)$ vs interface width d. Other parameters are the same as in Fig. 2

within the system. For smaller values of $d = 5$, the demixing between the two particle types is weak, resulting in shorter periods of time spent in the demixed state. Consequently, the system exhibits more frequent mixing-demixing events, as evident in Fig. 9(c)(I). As we increase the value of d, as shown in Fig. 9(c)(II–III), the particles demonstrate more substantial demixing behavior, leading to a reduction in the frequency of mixing-demixing events. However, when d is further increased, as observed in Fig. 9(c)(IV), the particles tend to phase separate less frequently, and it is hard to get the complete demixing. Our observations unveil an intriguing behavior within the range of interface widths (10, 15), where the two types of particles exhibit maximal phase separation, indicating a strong preference for spending more time in a demixed state than a mixed state.

While Fig. 9(c) clearly shows a decrease in the frequency of mixing-demixing events with increasing d for the intermediate range of d values. Whereas for large d values, the periodicity of mixing and demixing event weakens, and the periodic nature of the time series of $p(d)$ is no longer present.

To quantify how the particles' propensity for phase separation changes with varying interface width d, we present the plot of $P(d) = \langle p(d) \rangle$ as a function of junction width d in Fig. 10. Where $\langle .. \rangle$ stands for average over time in steady state as well as independent realizations. The plot of $P(d)$ against d clearly exhibits a peak at approximately $d \approx 14$. This peak aligns precisely with our earlier observation of maximal phase separation occurring within the range of $d =$ 12–15. Beyond this peak, $P(d)$ decreases, suggesting less prominent demixing of the two particle types, which further supports our findings. We performed additional tests with two other choices of random noise: $\phi \in (-1.2\pi, +0.8\pi)$ and $\phi \in (-0.8\pi, +1.2\pi)$ for the two types of particles, and remarkably, we obtained consistent results. Notably, the range of d where we observe maximum phase separation also coincides with the range where a transition to switching current inside the interface occurs. These collective findings provide valuable insights into the behavior of the system, highlighting the significance of the interface width and its impact on the demixing process and the occurrence of switching current behavior within the interface.

V. SUMMARY AND DISCUSSION

We have studied the properties of the collection of polar self-propelled particles moving on a two dimensional rectangular channel along an order-disorder interface with periodic boundary conditions in both directions. The interaction among the particles is taken as Vicsek type viz; particles move with constant speed and interact through short range alignment interaction. Inside the junction or disorder region, particles experience a high noise disorder state, and outside, they are in the ordered state. The width of the junction is adjusted by the junction width d. The model is motivated by the Josephson junction, an analogous equilibrium system in the solid state [49]. We studied the system for the two cases: (i) system WOP, where we do not impose any biased direction for moving SPPs, and (ii) system WP where a small external biased direction of motion along the long axis of the channel is introduced. Interestingly, the flock experiences more disturbance at wider junctions in the system WP in comparison to the system WOP. On increasing the width of the junction, the system WOP shows a very small change in the global orientation of particles, whereas the system WP shows a transition from an ordered to a disordered state. At the junction, we have found the current reversal for a range of intermediate widths of the junction. The current reversal is due to the reflection of particles from the walls of the interface. Such reflection is the response of a moving cluster when it experiences an abrupt change in thermal noise. The mechanism of reflection from the interface due to thermal noise is microscopically different from the reflection of particles from the hard walls of the obstacles in their path. But the result of the two reflection mechanisms is the same and leads to the reflection of an incoming cluster from the interface [53].

Further, we also modeled a binary mixture of the particles of two different types of chirality. We find that the two types of particles show macroscopic phase separation for the intermediate widths of the interface. Hence, such geometry can also be used for the sorting of different types of particles.

Interestingly, the study for SPPs at the interface has not been explored, although similar setups have been explored in experiments and theory for magnetic devices showing interesting properties [57,58]. A detailed comparison of our results obtained here with these studies is our future work. In our present study, an incoming particle experiences an abrupt temperature change, and we feel that such a change in temperature is responsible for the reversal in current. Whether a similar mechanism will be applicable to the case when we introduce a continuous thermal gradient or phoretic flow is an interesting project. On the basis of our present results on the abrupt thermal noise, we expect that for the phoretic flows, an incoming flock might penetrate to some distance and then can experience reflection or current reversal.

We believe that the results presented here can be tested in experiments by designing such a system. Our study also provides new scopes in active matter systems where particles experience different environments along their move.

The results presented here can be useful to understand the manufacturing of s variety of practical devices using biological agents: mechanical circuits, switching devices, geophysical sensors, etc.

ACKNOWLEDGMENTS

J.P.S., P.S.M., V.S., and S.M. thank PARAM Shivay for computational facility under the National Supercomputing Mission, Government of India, at the Indian Institute of Technology, Varanasi, and the computational facility at I.I.T. (BHU), Varanasi. P.S.M. thanks UGC for research fellowship. V.S. thanks DST INSPIRE (India) for the research fellowship. S.M. thanks DST, SERB (India), Projects No. CRG/2021/006945 and No. MTR/2021/000438 for financial support.

[1] F. Ndlec, T. Surrey, A. C. Maggs, and S. Leibler, Nature (London) **389**, 305 (1997).
[2] Y. Harada, A. Noguchi, A. Kishino, and T. Yanagida, Nature (London) **326**, 805 (1987).
[3] Y. Y. Toyoshima, S. J. Kron, E. M. McNally, K. R. Niebling, C. Toyoshima, and J. A. Spudich, Nature (London) **328**, 536 (1987).
[4] S. J. Kron and J. A. Spudich, Proc. Natl. Acad. Sci. USA **83**, 6272 (1986).
[5] M. T. Laub and W. F. Loomis, Mol. Biol. Cell **9**, 3521 (1998).
[6] J. Toner and Y. Tu, Phys. Rev. Lett. **75**, 4326 (1995).
[7] S. Pattanayak, J. P. Singh, M. Kumar, and S. Mishra, Phys. Rev. E **101**, 052602 (2020).
[8] T. Vicsek, A. Czirók, E. Ben-Jacob, I. Cohen, and O. Shochet, Phys. Rev. Lett. **75**, 1226 (1995).
[9] J. P. Singh and S. Mishra, Physica A **544**, 123530 (2020).
[10] P. K. Mishra and S. Mishra, Phys. Fluids **34**, 057110 (2022).
[11] J. P. Singh, S. Pattanayak, and S. Mishra, J. Phys. A: Math. Theor. **54**, 115001 (2021).
[12] M. C. Marchetti, J.-F. Joanny, S. Ramaswamy, T. B. Liverpool, J. Prost, M. Rao, and R. A. Simha, Rev. Mod. Phys. **85**, 1143 (2013).
[13] G. Grégoire and H. Chaté, Phys. Rev. Lett. **92**, 025702 (2004).
[14] H. Chaté, F. Ginelli, G. Grégoire, and F. Raynaud, Phys. Rev. E **77**, 046113 (2008).
[15] B. Bhattacherjee, S. Mishra, and S. S. Manna, Phys. Rev. E **92**, 062134 (2015).
[16] V. Narayan, S. Ramaswamy, and N. Menon, Science **317**, 105 (2007).
[17] C. Bechinger, R. Di Leonardo, H. Löwen, C. Reichhardt, G. Volpe, and G. Volpe, Rev. Mod. Phys. **88**, 045006 (2016).
[18] L. Angelani, R. Di Leonardo, and G. Ruocco, Phys. Rev. Lett. **102**, 048104 (2009).
[19] J. Harder, S. Mallory, C. Tung, C. Valeriani, and A. Cacciuto, J. Chem. Phys. **141**, 194901 (2014).
[20] S. Kumar, J. P. Singh, D. Giri, and S. Mishra, Phys. Rev. E **104**, 024601 (2021).
[21] P. de Castro and P. Sollich, Phys. Chem. Chem. Phys. **19**, 22509 (2017).
[22] V. Semwal, J. Prakash, and S. Mishra, arXiv:2112.13015 (2021)
[23] S. Pattanayak, R. Das, M. Kumar, and S. Mishra, Eur. Phys. J. E **42**, 62 (2019).
[24] V. Semwal, S. Dikshit, and S. Mishra, Eur. Phys. J. E **44**, 20 (2021).
[25] A. Baskaran and M. C. Marchetti, Phys. Rev. Lett. **101**, 268101 (2008).
[26] J. P. Singh, S. Pattanayak, S. Mishra, and J. Chakrabarti, J. Chem. Phys. **156**, 214112 (2022).
[27] I. Buttinoni, J. Bialké, F. Kümmel, H. Löwen, C. Bechinger, and T. Speck, Phys. Rev. Lett. **110**, 238301 (2013).
[28] M. E. Cates and J. Tailleur, Annu. Rev. Condens. Matter Phys. **6**, 219 (2015).
[29] E. Sese-Sansa, I. Pagonabarraga, and D. Levis, Europhys. Lett. **124**, 30004 (2018).
[30] S. Dikshit and S. Mishra, Eur. Phys. J. E **45**, 21 (2022).
[31] A. P. Solon, Y. Fily, A. Baskaran, M. E. Cates, Y. Kafri, M. Kardar, and J. Tailleur, Nat. Phys. **11**, 673 (2015).
[32] R. J. Hawkins, M. Piel, G. Faure-Andre, A. M. Lennon-Dumenil, J. F. Joanny, J. Prost, and R. Voituriez, Phys. Rev. Lett. **102**, 058103 (2009).
[33] S. Das, A. Garg, A. I. Campbell, J. Howse, A. Sen, D. Velegol, R. Golestanian, and S. J. Ebbens, Nat. Commun. **6**, 8999 (2015).
[34] W. Uspal, M. N. Popescu, S. Dietrich, and M. Tasinkevych, Soft Matter **11**, 434 (2015).
[35] G. Volpe, I. Buttinoni, D. Vogt, H.-J. Kümmerer, and C. Bechinger, Soft Matter **7**, 8810 (2011).
[36] A. Mozaffari, N. Sharifi-Mood, J. Koplik, and C. Maldarelli, Phys. Fluids **28**, 053107 (2016).
[37] G. P. Saracco, G. Gonnella, D. Marenduzzo, and E. Orlandini, Phys. Rev. E **84**, 031930 (2011).
[38] S. Mishra and S. Pattanayak, Physica A **477**, 128 (2017).
[39] E. Bodenschatz, W. Pesch, and G. Ahlers, Annu. Rev. Fluid Mech. **32**, 709 (2000).
[40] F. H. Busse and R. M. Clever, J. Fluid Mech. **91**, 319 (1979).
[41] A. Zumdieck, R. Voituriez, J. Prost, and J. Joanny, Faraday Discuss. **139**, 369 (2008).
[42] R. Voituriez, J.-F. Joanny, and J. Prost, Europhys. Lett. **70**, 404 (2005).
[43] X. Wang, M. In, C. Blanc, P. Malgaretti, M. Nobili, and A. Stocco, Faraday Discuss. **191**, 305 (2016).
[44] X. Wang, M. In, C. Blanc, M. Nobili, and A. Stocco, Soft Matter **11**, 7376 (2015).
[45] A. Dominguez, P. Malgaretti, M. Popescu, and S. Dietrich, Soft Matter **12**, 8398 (2016).
[46] P. Malgaretti, M. Popescu, and S. Dietrich, Soft Matter **12**, 4007 (2016).
[47] K. Dietrich, D. Renggli, M. Zanini, G. Volpe, I. Buttinoni, and L. Isa, New J. Phys. **19**, 065008 (2017).
[48] T. Kontos, M. Aprili, J. Lesueur, F. Genêt, B. Stephanidis, and R. Boursier, Phys. Rev. Lett. **89**, 137007 (2002).
[49] B. D. Josephson, Phys. Lett. **1**, 251 (1962).
[50] A. I. Buzdin, L. Bulaevskii, and S. Panyukov, Zh. Eksp. Teor. Fiz., Pis'ma **35**, 147 (1982) [JETP Lett. **35**, 178 (1982)].
[51] T. Kontos, M. Aprili, J. Lesueur, and X. Grison, Phys. Rev. Lett. **86**, 304 (2001).
[52] I. Kulik, J. Exptl. Theoret. Phys. (U.S.S.R.) **49**, 1211 (1965) [Sov. Phys. JETP **22**, 841 (1966)].
[53] J. Codina, B. Mahault, H. Chaté, J. Dobnikar, I. Pagonabarraga, and X. Q. Shi, Phys. Rev. Lett. **128**, 218001 (2022).
[54] J. P. Singh, S. Kumar, and S. Mishra, J. Stat. Mech.: Theory Exp. (2021) 083217.

[55] S. Mishra, A. Baskaran, and M. C. Marchetti, Phys. Rev. E **81**, 061916 (2010).

[56] See Supplemental Material at http://link.aps.org/supplemental/10.1103/PhysRevE.108.034608 for the interaction between the particle cluster and the interface, including the reflection phenomena, takes place between the 11 s and 1 min marks within the video (SM1_I.mp4);for the interaction between the particle cluster and the interface, including the reflection phenomena, takes place between the 36 s and 1 min 51 s marks within the video (SM1_II.mp4); for illustrative video. Starting from the 6 s mark in the video, we can observe the interaction between the particle cluster and the interface (SM2.mp4).

[57] R. Gurzhi, A. Kalinenko, A. Kopeliovich, A. Yanovsky, E. Bogachek, and U. Landman, J. Supercond. **16**, 201 (2003).

[58] G. Schmidt, G. Richter, P. Grabs, C. Gould, D. Ferrand, and L. W. Molenkamp, Phys. Rev. Lett. **87**, 227203 (2001).